HHS Public Access

Author manuscript

Cancer Immunol Res. Author manuscript; available in PMC 2019 August 01.

Published in final edited form as:

Cancer Immunol Res. 2018 August ; 6(8): 900–909. doi:10.1158/2326-6066.CIR-17-0270.

Primary T cells from cutaneous T-cell lymphoma skin explants display an exhausted immune checkpoint profile

Christiane Querfeld[1,2,8,9], **Samantha Leung**[1], **Patricia L. Myskowski**[2,8], **Shane A. Curran**[1], **Debra A. Goldman**[6], **Glenn Heller**[6], **Xiwei Wu**[9], **Sung Hee Kil**[9], **Sneh Sharma**[1], **Kathleen J. Finn**[1], **Steven Horwitz**[3,8], **Alison Moskowitz**[3,8], **Babak Mehrara**[5,8], **Steven T. Rosen**[9], **Allan C. Halpern**[2,8], and **James W. Young**[1,4,7,8]

[1]Laboratory of Cellular Immunobiology, Immunology Program, Sloan Kettering Institute for Cancer Research, Memorial Sloan Kettering Cancer Center

[2]Dermatology Service, Memorial Sloan Kettering Cancer Center

[3]Lymphoma Service, Memorial Sloan Kettering Cancer Center

[4]Adult Bone Marrow Transplant Service, Dept. of Medicine, Memorial Sloan Kettering Cancer Center

[5]Plastic and Reconstructive Surgery Service, Dept. of Surgery, Memorial Sloan Kettering Cancer Center

[6]Department of Epidemiology and Biostatistics, Memorial Sloan Kettering Cancer Center

[7]The Rockefeller University, New York, New York, 10065

[8]Weill Cornell Medical College, New York, New York, 10065

[9]Beckman Research Institute, City of Hope, Duarte, CA, USA

Abstract

Cutaneous T-cell lymphoma (CTCL) develops from clonally expanded $CD4^+$ T cells in a background of chronic inflammation. Although dendritic cells (DCs) stimulate T cells and are present in skin, cutaneous T cells in CTCL do not respond with effective antitumor immunity. We evaluated primary T-cell and DC émigrés from epidermal and dermal explant cultures of skin biopsies from CTCL patients ($n = 37$) and healthy donors ($n = 5$). Compared with healthy skin, $CD4^+$ CTCL populations contained more T cells expressing PD-1, CTLA-4, and LAG-3. $CD8^+$ CTCL populations contained more T cells expressing CTLA-4 and LAG-3. CTCL populations also contained more T cells expressing the inducible T-cell costimulator (ICOS), a marker of T-cell activation. DC émigrés from healthy or CTCL skin biopsies expressed PD-L1, indicating that maturation during migration resulted in PD-L1 expression irrespective of disease. Most T cells did not express PD-L1. Using skin samples from 49 additional CTCL patients for an unsupervised analysis of genome-wide mRNA expression profiles corroborated that advanced T3/T4-stage

CORRESPONDING AUTHOR and CURRENT ADDRESS: Christiane Querfeld, MD, PhD; Toni Stephenson Lymphoma Center, Dept. of Pathology and Div. of Dermatology, City of Hope, 1500 E. Duarte Rd., Duarte, CA, 91010. Phone 626-256-4673. Fax 626-301-8136. cquerfeld@coh.org.

CONFLICTS OF INTEREST: The authors have no conflicts of interest to disclose.

samples expressed more checkpoint inhibition mRNA compared with T1/T2 stage patients or healthy controls. Exhaustion of activated T cells is therefore a hallmark of both $CD4^+$ and $CD8^+$ T cells isolated from the lesional skin of patients with CTCL, with increasing expression as the disease progresses. These results justify identification of antigens driving T-cell exhaustion and the evaluation of immune checkpoint inhibition to reverse T-cell exhaustion earlier in the treatment of CTCL.

Keywords

T-cell exhaustion; immune checkpoint; cutaneous T-cell lymphoma; dendritic cell; Langerhans cell

INTRODUCTION

Cutaneous T-cell lymphomas (CTCL) comprise a set of related malignancies characterized by the accumulation of neoplastic memory T cells in the skin in a background of chronic inflammation. The most common subtypes of CTCL are mycosis fungoides (MF) and Sézary syndrome (SS), the advanced stages of which have an estimated 5-year overall survival of 24% (1,2). There is no cure and patients frequently relapse, requiring repeated treatment courses for disease control.

The lack of a clear understanding of CTCL etiology has impeded therapeutic advances toward disease-free and overall survival. Although dendritic cell (DC) subsets populate all cutaneous and mucosal surfaces in both the steady state and inflammation (3), and irrespective of the presence of tumor-infiltrating $CD8^+$ T cells in the CTCL lesions, clonally expanded malignant $CD4^+$ T-cell clones persist in chronically inflamed skin. This observation suggests that chronic inflammation in the tumor microenvironment is ineffective or may even impair successful antitumor immunity mediated by the $CD8^+$ T cells (4,5).

The type and duration of signals encountered by naïve T cells at the time of antigen presentation by DCs determine T-cell activation and immune responsiveness. During initial antigen sensitization, T cells express the T-cell receptor (TCR) for DC-presented antigen along with costimulatory receptors that bind DC costimulatory ligands and cytokines, all of which in concert ensure the initiation of effective T-cell effector responses (6,7). T cells in turn express compensatory immune checkpoint receptors, which dampen an otherwise unchecked immune response (8–10). In tumors that express self-differentiation antigens or during chronic viral infections, however, chronic or excessive T-cell stimulation can lead to overexpression of inhibitory checkpoint receptors. Ligand binding to these receptors, which include PD-1, LAG-3, TIM-3, CTLA-4, and others, can elicit a survival maneuver termed T-cell exhaustion, whereby chronically overactivated T cells neither transition to memory T cells nor undergo apoptosis or deletion. Instead, these exhausted T cells enter a potentially reversible state of unresponsiveness toward pathogens or tumor antigens (11,12). The functional consequences are impaired immune surveillance and unchecked viral persistence or tumor growth. Antibody-based drugs that block these checkpoint inhibitors can reverse T-cell exhaustion, a therapeutic approach that has revolutionized treatment of multiple cancers, especially in patients who have evidence of a prior immune response.

The rarity of CTCL and the lack of robust methods for isolating tumor cells directly from involved skin have limited translational investigations to optimize control or cure. Results from immunohistochemical analyses of T-cell immune checkpoint markers (13–16) have been inconclusive due to limitations imposed by the small number of distinguishable antibodies and fluorochromes available for simultaneous evaluation of checkpoint inhibition epitopes.

We therefore used multicolor flow cytometry to analyze primary T-cell and DC émigrés in liquid culture medium (17,18) from ~36h skin explant cultures of separated epidermis and dermis from lesional and healthy skin. These studies were complemented by unsupervised genome-wide mRNA sequencing, as well as multiplex immunohistochemistry, using checkpoint markers restricted to PD-1 and PD-L1 because of the limitations noted above. Our goal was to evaluate immune checkpoint expression as a marker of T-cell dysregulation across the continuum of CTCL disease stages in order to develop a rationale for identifying antigens responsible for chronic T-cell overstimulation and to guide use of checkpoint inhibitors earlier in the treatment of CTCL.

MATERIALS AND METHODS

Study population and tissue samples

Lesional skin shave biopsies (approximately 1–1.5 cm) were obtained under local anesthesia from 37 CTCL outpatients (23 males and 14 females; median age 57 years; range, 24–86 years) seen at the Memorial Sloan Kettering Cancer Center (MSKCC) Multidisciplinary Cutaneous Lymphoma Clinic (Table 1). Additional skin from the same biopsy area was submitted for routine histopathology and immunohistochemistry, by which each biopsy was confirmed as MF and classified as patch, plaque, or tumor lesion. Diagnosis of SS required additional confirmation of circulating Sézary cells (≥1,000 cell/μL) with immunophenotypic abnormalities by standard flow cytometry (19). Additional samples included intact lesional skin biopsies in the CTCL tissue bank at the City of Hope (COH), used for unsupervised genome-wide mRNA sequencing and 6-color multiplex immunohistochemistry for immune checkpoint expression.

Immunohistochemistry for diagnostic confirmation of CTCL and tumor stage most commonly revealed an aberrant $CD3^+$ $CD4^+CD8^-$ phenotype with loss or partial loss of CD7 expression. Samples non-diagnostic for MF were excluded. We characterized each patient according to the 2005 WHO-EORTC diagnosis and classification criteria (1). We then performed clinical staging according to the revised staging system for CTCL, based on the tumor-node-metastasis-blood (TNMB) classification system (20). We assigned tumor burden based on skin involvement. T1 or T2 respectively defined patches/plaques involving < 10% or ≥ 10% of body surface area (BSA). T3 required ≥ 1 skin tumor, and T4 necessitated generalized erythroderma. This staging also applied to the few patients with Sézary syndrome, defined by leukemic involvement of the cancerous T cells in addition to their presence in skin tumors. Thirty-seven patients provided biopsies in the following categories: clinical stage IA/IB, $n = 20$ (T1 + T2); stage IIA, $n = 1$ (T2); stage IIB, $n = 7$ (T3); stage IIIB, $n = 3$ (T4); stage IVA, $n = 5$ (T4); and stage IVB, $n = 1$ (T4). Five patients

undergoing reconstructive plastic surgery after successful treatment of breast cancer provided healthy skin.

Forty-nine formalin-fixed, paraffin-embedded (FFPE), and histologically confirmed lesional skin biopsies from 45 distinct CTCL patients identified from the City of Hope (COH) CTCL tissue bank underwent unsupervised genome-wide mRNA sequencing. Stages included T1 (n = 7), T2 (n = 16), T3 (n = 18), and T4 (n = 4). Three FFPE tissue samples of healthy skin from 3 patients undergoing reconstructive plastic surgery served as controls.

All patient tissue collection and research use adhered to protocols approved by the Institutional Review and Privacy Boards at MSKCC and COH, in accordance with the Declaration of Helsinki. All participants signed written informed consents.

Cell isolation and preparation

Fresh skin samples cut into small pieces were incubated for 30 min at 37°C in 5% CO_2 in DMEM/F-12 (Stem Cell Technologies, Cambridge, MA) with dispase II (1 IU/ml, Roche Diagnostics, Indianapolis, IN) to facilitate separation of the epidermis from the dermis. The epidermis was peeled away from the dermis, after which each was placed in separate suspension cultures (Costar) in RPMI 1640 medium with 10 mM HEPES, 1% penicillin/streptomycin (Media Lab, MSKCC), 50 mM L-glutamine (Cellgro, Manassas, VA), 50 μM 2-mercaptoethanol (Gibco, Life Technologies, Carlsbad, CA), and 10% heat-inactivated pooled healthy human serum (Atlanta Biologicals, Flowery Branch, GA) at 37°C in 5% CO_2 (17,18). Cells were collected separately from epidermal and dermal explant culture medium after 36 h migration into the medium. Medium never contained fetal calf serum to avoid artifactual background activation of DC émigrés as a result of bystander stimulation of T-cell crawlouts reacting against DC-presented xenogeneic serum proteins. T cells and DCs were manually counted based on distinct morphologies using a hemocytometer.

T-cell and dendritic cell phenotyping by flow cytometry

Migrated skin cells were stained with fluorochrome-conjugated monoclonal antibodies and analyzed on an LSR Fortessa (Becton Dickinson, Franklin Lakes, New Jersey) flow cytometer. The following antibodies were used: anti-CD3 (BV650, Biolegend 317324, San Diego, CA), anti-CD8 (BV785, Biolegend 301046), anti-CD4 (PE-Texas Red, Life Technologies MHCDO417), anti-PD-1 (PerCP-Cy5.5, eBioscience 46-2799, San Diego, CA), anti-LAG-3 (APC, eBioscience 17-2239), anti-ICOS (PE-Cy7, eBioscience 25-9948), anti-TIM-3 (Alexa Fluor 700, R&D Systems FAB2365N, Minneapolis, MN), anti-CTLA-4 (PE-Cy5, BD Pharmingen 555854, Franklin Lakes, NJ), anti-PD-L1 (PE, BD Pharmingen 557924), anti-CD1a (PE-Cy5, BD Pharmingen 555808), anti-CD11b (PE-Cy7, BD Pharmingen 557743), anti-CD11c (APC, BD Pharmingen 559877 and Alexa Fluor 700, BD Pharmingen 561352), anti-CD14 (FITC, BD Pharmingen 555397; PE-Cy7, BD Pharmingen 557742; and BV785, Biolegend 301839), and anti-HLA-DR (ECD, Beckman Coulter IM3636, Brea, CA, and PE-Cy7, BD Pharmingen 335795). T-cell numbers were sufficient to use nonreactive isotype-matched controls to determine gating of negative vs positive events. In contrast,]too few DCs from these small shave biopsies were left after nonspecific losses during staining and washing. We instead used unstained cells to determine negative gates,

given that positive fluorescence was always definitive for the markers studied. The LIVE / DEAD Fixable Aqua Dead Cell Stain Kit (Life Technologies) excluded dead cells, so that gates were set for collection and analysis of at least 10,000 live events. Data were analyzed with FlowJo 9.7.6 software (TreeStar, Ashland, OR). T-cell analyses included viable events that were positive for CD3 and either CD4 or CD8 to capture the respective T-cell subsets. Analyses of cutaneous DC crawlouts after live gating included the following subsets: epidermal Langerhans cells (LCs) ($CD1a^+$, $CD14^{neg}$, $HLA\text{-}DR^{bright}$), dermal $CD1a^+$ DCs ($CD1a^+$, $CD14^{neg}$, $HLA\text{-}DR^{bright}$, $CD11b^+$, $CD11c^+$), and dermal $CD14^+$ DCs ($CD1a^{neg}$, $CD14^+$, $HLA\text{-}DR^{bright}$, $CD11b^+$, $CD11c^+$) (21,22).

RNA sequencing, library preparation, and data analysis

Total RNA from formalin-fixed paraffin-embedded (FFPE) skin from healthy controls and CTCL patients was extracted with miRNeasy FFPE kit (Qiagen). Total RNA was rRNA-depleted with the Ribo-Zero low input kit for Human/Mouse/Rat (Illumina, San Diego, USA) using 300ng of starting material. RNAseq libraries were prepared from Ribo-Zero mRNA-enriched material using KAPA Stranded RNA-Seq Library Preparation Kit (Illumina Platforms) (Kapa Biosystems, Wilmington, USA) and 10 cycles of PCR amplification. Libraries were purified using AxyPrep Mag PCR Clean-up kit (Thermo Fisher Scientific, Waltham, MA). Each library was quantified using a Qubit fluorometer (Life Technologies), and the size distribution was assessed using the 2100 Bioanalyzer (Agilent Technologies, Santa Clara, USA). Sequencing was performed on an Illumina Hiseq 2500 (Illumina, San Diego, CA, USA) instrument using the TruSeq PE Cluster Kit V4-cBot-HS (Illumina®) to generate 101 bp paired-end reads sequencing with v4 chemistry. Quality control of RNA-Seq reads used FastQC. These data sets are deposited in the Gene Expression Omnibus (GEO) repository under the accession number GSE113113.

Immunohistochemical evaluation of intact CTCL skin biopsies

Intact FFPE skin biopsies from the COH CTCL tissue bank were sectioned and subjected to standard immunohistochemical evaluation. Despite limitations imposed by antigen specificities of available reagents with non-overlapping isotypes, secondary antibodies, and/or fluorochromes, we evaluated PD-1 and PD-L1 expression by $CD4^+$ and $CD8^+$ T cells.

Data and statistical analyses

The Wilcoxon rank sum test assessed the significance of differences in expression of T-cell exhaustion markers between healthy skin versus all samples from lesional CTCL skin (Table 2). The significance threshold was $P = 0.05$, and all tests were two-sided. All analyses of percentages obtained from flow cytometric data were plotted and calculated using Prism 6 software (GraphPad, La Jolla, CA). The Mann-Whitney U test compared the significance of differences in the mean fluorescent intensity (MFI) of PD-L1 expressed by DC subtypes isolated from healthy vs lesional CTCL skin.

The RNA-Seq reads were aligned to hg19 genome assembly using Tophat2 with default settings, and gene expression levels of Refseq genes were counted with customized R scripts. The expression data were normalized using the trimmed mean of M values (TMM) method, implemented in the Bioconductor package “edgeR” to obtain counts per million

(CPM) and then scaled by gene length in kb. The normalized expression values were log2 transformed with offset of 1 and filtered to retain 6,418 genes with log2 expression value ≥ 1 in at least 5 samples and standard deviation ≥ 0.5. The normalized log2 expression values of these filtered genes or selected immune checkpoint and inflammatory genes were mean centered and subjected to hierarchical clustering using Cluster 3.0 with Pearson correlation distance and complete linkage. The clustering results were visualized using Java Treeview.

RESULTS

Increased immune checkpoint expression in T-cell crawlouts from lesional CTCL skin

These studies demonstrate that the epidermal $CD3^+CD4^+$ population across all CTCL stages displayed a statistically significant increase in the percent expression of CTLA-4 ($P = 0.005$), ICOS ($P = 0.001$), LAG-3 ($P = 0.007$), and PD-1 ($P = 0.001$), but not PD-L1 or TIM-3 (Fig. 1A and Table 2; Supplementary Fig. S1), compared with the same cell types from healthy skin. For dermal $CD3^+CD4^+$ T cells, expression across all CTCL samples was significantly higher than healthy skin only for PD-1 ($P = 0.031$; Fig. 1B, Table 2). Expression of CTLA-4, ICOS, LAG-3, PD-L1, and TIM-3 did not reach significance among the dermal $CD3^+CD4^+$ T-cell crawlouts from CTCL lesional skin, compared with those from healthy control dermis. Our finding that 60–80% of epidermal and dermal $CD4^+$ T cells from lesional CTCL skin expressed PD-1 aligns with or exceeds prior reports for MF (13,14). These increases in expression occurred even in the early stages of CTCL.

Similar to the $CD3^+CD4^+$ population, the epidermal $CD3^+CD8^+$ T-cell émigrés across all stages of CTCL expressed significantly higher levels of CTLA-4 ($P = 0.004$), ICOS ($P = 0.004$), and LAG-3 ($P = 0.008$), but not PD-1, PD-L1, or TIM-3, compared with healthy control skin (Fig. 1C, Table 2). Dermal $CD3^+CD8^+$ T-cell crawlouts displayed significantly higher levels of CTLA-4 ($P = 0.018$), ICOS ($P = 0.048$), and TIM-3 ($P = 0.006$), but not LAG-3, PD-1, or PD-L1 for all stages of CTCL, compared with healthy control dermis (Fig. 1D, Table 2).

PD-L1 levels in DCs from healthy epidermis and lesional CTCL skin are comparable

Because DCs initiate T cell–mediated immunity, we examined PD-L1 expression in three phenotypically defined subsets of cutaneous DC émigrés: $HLA\text{-}DR^+$, $CD1a^+$, $CD14^{neg}$ epidermal LCs; $HLA\text{-}DR^+$, $CD11b^+$, $CD11c^+$, $CD1a^+$, $CD14^{neg}$ dermal DCs; and $HLA\text{-}DR^+$, $CD11b^+$, $CD11c^+$, $CD1a^{neg}$, $CD14^+$ dermal DCs (21,22). LC and DC yields were lower than T-cell yields (Supplementary Table S1), thereby allowing adequate numbers of cells only from 3 control and 3 CTCL lesional skin biopsies. DCs number 1% or fewer of the total leukocytes in healthy blood and most tissues, yet DCs comprise almost 100% of the rare leukocytes present in healthy epidermis. The presence of other leukocytes in the epidermis is therefore pathologic. Émigrés of each cutaneous dendritic cell subtype from control and CTCL skin expressed comparable and expected phenotypes for gating by flow cytometry, as well as similar levels of PD-L1 (Fig. 2), although the lesional skin-derived T cells from CTCL patients expressed increased PD-1 compared with controls.

Expression of T-cell exhaustion genes increases with increasing disease stage

RNAseq analysis of 49 independent lesional skin FFPE samples from the COH CTCL tissue bank was performed to determine mRNA expression profiles in CTCL (Fig. 3A, B). CTCL samples were divided into 2 groups (decreased/low and increased/high levels) according to gene expression patterns. The unsupervised hierarchical clustering analysis identified mRNA expression patterns characteristic of early stage MF (T1/T2), advanced stage MF/SS (T3/T4) samples, and healthy skin (Fig. 3A). Data shown are $\log_2$ (fold change) relative to the median expression across all samples. Genes in rows and samples in columns were hierarchically clustered. Samples were arranged by sample type with the following sample categories assigned by color: healthy control (light blue), T1 stage (blue), T2 stage (black), T3 stage (ochre) and T4 stage (yellow). Five gene clusters were identified with gene ontology (GO) annotation analysis based on the basis of their related functions. Cluster 1 highlights genes related to inflammatory response, T-cell activation, and inhibition/exhaustion, with a different gene expression profile observed in advanced stage MF/SS (T3/T4) samples compared with those of early stage (T1/T2) samples. RNAseq analysis of these archival tissues used total RNA isolated from skin sections. Clusters 2–5 therefore reflect other components of the cutaneous microenvironment: (2) epidermis and keratinocyte development, (3) extracellular matrix regulation, (4) neutrophil degranulation; negative regulation of transcription, and (5) innate immune response. All of these clusters displayed differentially expressed profiles for T1/T2 stage compared with advanced T3/T4 stage.

To elucidate whether MF/SS display an exhaustion-related marker expression profile from cluster 1 different from that of healthy skin, we performed a supervised analysis following the previously mentioned criteria (Fig. 3B). Immune checkpoint and inflammatory gene expression profiling [PDCD1 (PD-1), CD274 (PD-L1), HAVCR2 (TIM3), CTLA4, LAG3, ICOS, IFNG, FOXP3 and IL10] were performed. Clustering analysis divided CTCL skin samples into two groups based on low/decreased vs increased/high expression of gene sets associated with immune checkpoints and inflammation. Advanced stages (T3/T4) displayed higher gene expression for immune checkpoints and inflammation compared than did T1/T2 stage patients or healthy controls. In addition, the expression profiles corroborated our phenotypic analyses of immune checkpoint receptors by flow cytometry. For mRNA transcripts of IFNG, FOXP3, and IL10, higher expression correlated with advanced T3/T4 stage disease (23).

Multicolor immunohistochemistry of CTCL lesions

Immunohistochemistry (IHC) of intact FFPE sections (Supplementary Fig. S2) revealed the expected epidermotropic and dense dermal atypical lymphoid infiltrate interspersed with morphologic histiocyte-type cells that include some inflammatory DCs. The atypical lymphocytes were $CD3^+CD4^+CD7^-CD8^-$. Multicolor IHC of a representative patient with plaques (T2) and another patient with tumor lesion (T3) demonstrated colocalization of PD-1 with CD3, CD4, and CD8 expression (Figs. 4 and 5). As the atypical CTCL lymphocytes lacked CD8, the observed $CD8^+$ T cells, by exclusion, must represent infiltrating and potentially reactive CTLs expressing the inhibitory PD-1 epitope. Infiltrates in tumor lesions (T3) expressed more PD-1 and PD-L1 than did infiltrates in plaque (T2)

disease (200x magnification; insets represent 400x magnification of small regions of multiplex images).

DISCUSSION

This study reports the immunophenotype of primary T cells and DC subsets isolated directly from 1–1.5 cm^2 shave biopsies of lesional skin from CTCL patients and compared with the immunophenotypes of T-cell and DC émigrés from healthy skin. Given the epidermotrophic nature of CTCL, skin explant cultures of separated epidermal and dermal sheets (17,18) permitted characterization of T-cell and DC émigrés from each skin layer for phenotypic and molecular analyses. We evaluated patients according to tumor staging (T1 + T2, T3, and T4), but the few samples from patients with the most advanced disease necessitated immunophenotypic comparisons of healthy skin vs skin from all CTCL stages combined. In contrast, gene expression profiling demonstrated positive correlations between increased checkpoint inhibitor expression and higher disease stage.

Other investigators have used skin explant cultures of epidermal sheets and dermis (17,18). Here we characterized primary immune cells of CTCL in lesional skin. Our approach avoids problems caused by poor enzymatic digestion of the cutaneous extracellular matrix, long-term culture, or use of cell lines derived from malignant, epidermotrophic $CD4^+$ T cells. Our skin explant cultures require mechanical manipulation, which activates DC subtypes as émigrés into the culture medium. We used 10% pooled normal human serum and limited exposure to approximately 36 hrs, thus avoiding exposure to fetal calf serum or cytokines and bystander acfivation of DCs that could stimulate T cells against xenogeneic peptides. The DC and T-cell crawlouts we analyzed remained close to their *in situ* state, thus facilitating phenotypic characterization by flow cytometry and better phenotypic characterization than feasible with use of immunohistochemistry of tissue sections. Because the cell populations stained with monoclonal antibodies to immune checkpoint markers are compared against isotype-matched (or unstained, in the case of DCs) controls, determining positive expression is straightforward and avoids the challenges of interpreting immunohistochemical staining of tissue (15).

Although the pattern of immune checkpoint epitope expression of epidermal T cells approximated that of dermal T cells, the disease-associated increase was not as pronounced in the dermis. This finding may reflect a mixture of malignant and nonmalignant cells in the dermal compartment, but it is most compatible with the epidermotropic nature of CTCL. The gene expression data corroborate the association between increased expression of checkpoint inhibitors and more advanced tumor stage.

External antigens in the epidermis may also increase expression of the exhausted phenotype. Studies have not yet established a causal link, however, between the exhausted phenotype we report here and any specific antigen(s) driving chronic overstimulation, clonal expansion, and malignant transformation (24). Newer molecular methods, including high-throughput sequencing modalities, are revolutionizing our understanding of the microbiome and its relationship with disease and clinical treatment outcomes (25,26). Such approaches may clarify why CTCL lesions have a high number of exhausted T cells, given that the skin has

typical numbers of potent antigen-presenting and immunostimulatory DCs. The process of exhaustion may also involve increasing mutational load, as reported for CTCL, characterized by somatic mutations in genes involved in T-cell signaling, activation, and apoptosis, as well as chromatin remodeling and responses to DNA damage (27). Increasing mutational load generates multiple tumor neoantigens, which can in turn exacerbate T-cell exhaustion, rendering any $CD8^+$ antitumor CTLs ineffective without the addition of immune checkpoint blockade.

A limitation to progress in CTCL is the rarity of the disorder. Obtaining skin biopsies of CTCL lesions from outpatients is feasible only under local anesthesia and yields only small specimens. Although the flow cytometry-based assessment of primary T-cell and DC crawlouts permits concurrent analysis of multiple markers, the limited cell numbers derived from the skin biopsies in this study precluded complementary functional assays of T-cell responsiveness. Another challenge is that apart from atypical morphology and the usual loss of CD7, there is no pathognmonic epitope that can distinguish malignant $CD4^+$ T cells from benign $CD4^+$ T cells in the infiltrate. Single-cell RNA sequencing focused on TCR α/β VDJ rearrangements with additional phenotypic markers may provide a strategy to identify clonal T cells in conjunction with phenotypic investigations (28–31). Nevertheless, our immunophenotypic and gene expression profile findings represent advances in understanding the pathophysiology of this uncommon lymphoma. These results provide a rationale to identify culprit antigens in an altered cutaneous microbiome driving T-cell exhaustion and to evaluate immune checkpoint inhibition to reverse T-cell exhaustion earlier in the treatment of this disease. We anticipate that this work will therefore facilitate the mechanistic discovery and development of more effective therapies for CTCL.

Supplementary Material

Refer to Web version on PubMed Central for supplementary material.

Acknowledgments

FINANCIAL SUPPORT: This research was funded in part through National Institutes of Health (NIH)/National Cancer Institute (NCI) Cancer Center Support Grant (P30CA033572) to the City of Hope; NIH/NCI Cancer Center Support Grant (P30CA08748) to MSKCC; The Ted Schwartz Family Foundation to CQ; NCI/NIH grant P01CA23766 to JWY; and Swim Across America Long Island Sound Chapter to JWY.

Nancy Linford, Ph.D. and James Sanchez, Ph.D. (City of Hope) provided editorial assistance for this manuscript.

References

1. Willemze R, Jaffe ES, Burg G, Cerroni L, Berti E, Swerdlow SH, et al. WHO-EORTC classification for cutaneous lymphomas. Blood. 2005; 105(10):3768–85. [PubMed: 15692063]
2. Criscione VD, Weinstock MA. Incidence of cutaneous T-cell lymphoma in the United States, 1973–2002. Arch Dermatol. 2007; 143(7):854–9. [PubMed: 17638728]
3. Klechevsky E. Functional Diversity of Human Dendritic Cells. Adv Exp Med Biol. 2015; 850:43–54. [PubMed: 26324345]
4. Berger CL, Wang N, Christensen I, Longley J, Heald P, Edelson RL. The immune response to class I-associated tumor-specific cutaneous T-cell lymphoma antigens. J Invest Dermatol. 1996; 107(3): 392–7. [PubMed: 8751976]

5. Bagot M, Nikolova M, Schirm-Chabanette F, Wechsler J, Boumsell L, Bensussan A. Crosstalk between tumor T lymphocytes and reactive T lymphocytes in cutaneous T cell lymphomas. Ann N Y Acad Sci. 2001; 941:31–8. [PubMed: 11594580]
6. Young JW, Koulova L, Soergel SA, Clark EA, Steinman RM, Dupont B. The B7/BB1 antigen provides one of several costimulatory signals for the activation of CD4+ T lymphocytes by human blood dendritic cells in vitro. J Clin Invest. 1992; 90(1):229–37. [PubMed: 1378854]
7. Carreno BM, Collins M. The B7 family of ligands and its receptors: new pathways for costimulation and inhibition of immune responses. Annu Rev Immunol. 2002; 20:29–53. [PubMed: 11861596]
8. Smith-Garvin JE, Koretzky GA, Jordan MS. T cell activation. Annu Rev Immunol. 2009; 27:591–619. [PubMed: 19132916]
9. Chen L, Flies DB. Molecular mechanisms of T cell co-stimulation and co-inhibition. Nat Rev Immunol. 2013; 13(4):227–42. [PubMed: 23470321]
10. Freeman GJ, Long AJ, Iwai Y, Bourque K, Chernova T, Nishimura H, et al. Engagement of the PD-1 immunoinhibitory receptor by a novel B7 family member leads to negative regulation of lymphocyte activation. J Exp Med. 2000; 192(7):1027–34. [PubMed: 11015443]
11. Schietinger A, Greenberg PD. Tolerance and exhaustion: defining mechanisms of T cell dysfunction. Trends Immunol. 2014; 35(2):51–60. [PubMed: 24210163]
12. Wherry EJ, Blattman JN, Murali-Krishna K, van der Most R, Ahmed R. Viral persistence alters CD8 T-cell immunodominance and tissue distribution and results in distinct stages of functional impairment. J Virol. 2003; 77(8):4911–27. [PubMed: 12663797]
13. Wada DA, Wilcox RA, Harrington SM, Kwon ED, Ansell SM, Comfere NI. Programmed death 1 is expressed in cutaneous infiltrates of mycosis fungoides and Sezary syndrome. Am J Hematol. 2011; 86(3):325–7. [PubMed: 21328438]
14. Cetinozman F, Jansen PM, Vermeer MH, Willemze R. Differential expression of programmed death-1 (PD-1) in Sezary syndrome and mycosis fungoides. Arch Dermatol. 2012; 148(12):1379–85. [PubMed: 23247480]
15. Cetinozman F, Jansen PM, Willemze R. Expression of programmed death-1 in skin biopsies of benign inflammatory vs. lymphomatous erythroderma. Brit J Dermatol. 2014; 171(3):499–504. [PubMed: 24601935]
16. Kantekure K, Yang Y, Raghunath P, Schaffer A, Woetmann A, Zhang Q, et al. Expression patterns of the immunosuppressive proteins PD-1/CD279 and PD-L1/CD274 at different stages of cutaneous T-cell lymphoma/mycosis fungoides. The Am J Dermatopathol. 2012; 34(1):126–8. [PubMed: 22094231]
17. Pope M, Betjes MG, Hirmand H, Hoffman L, Steinman RM. Both dendritic cells and memory T lymphocytes emigrate from organ cultures of human skin and form distinctive dendritic-T-cell conjugates. J Invest Dermatol. 1995; 104(1):11–7. [PubMed: 7798627]
18. Stoitzner P, Romani N, McLellan AD, Tripp CH, Ebner S. Isolation of skin dendritic cells from mouse and man. Methods Mol Biol. 2010; 595:235–48. [PubMed: 19941117]
19. Olsen E, Vonderheid E, Pimpinelli N, Willemze R, Kim Y, Knobler R, et al. Revisions to the staging and classification of mycosis fungoides and Sezary syndrome: a proposal of the International Society for Cutaneous Lymphomas (ISCL) and the cutaneous lymphoma task force of the European Organization of Research and Treatment of Cancer (EORTC). Blood. 2007; 110(6):1713–22. [PubMed: 17540844]
20. Olsen EA, Whittaker S, Kim YH, Duvic M, Prince HM, Lessin SR, et al. Clinical end points and response criteria in mycosis fungoides and Sezary syndrome: a consensus statement of the International Society for Cutaneous Lymphomas, the United States Cutaneous Lymphoma Consortium, and the Cutaneous Lymphoma Task Force of the European Organisation for Research and Treatment of Cancer. J Clin Oncol. 2011; 29(18):2598–607. [PubMed: 21576639]
21. Klechevsky E, Morita R, Liu M, Cao Y, Coquery S, Thompson-Snipes L, et al. Functional specializations of human epidermal Langerhans cells and CD14+ dermal dendritic cells. Immunity. 2008; 29(3):497–510. [PubMed: 18789730]
22. Collin M, McGovern N, Haniffa M. Human dendritic cell subsets. Immunology. 2013; 140(1):22–30. [PubMed: 23621371]

23. Asadullah K, Docke WD, Haeussler A, Sterry W, Volk HD. Progression of mycosis fungoides is associated with increasing cutaneous expression of interleukin-10 mRNA. J Invest Dermatol. 1996; 107(6):833–7. [PubMed: 8941670]
24. Mirvish JJ, Pomerantz RG, Falo LD Jr, Geskin LJ. Role of infectious agents in cutaneous T-cell lymphoma: facts and controversies. Clin Dermatol. 2013; 31(4):423–31. [PubMed: 23806159]
25. Lipkin WI, Anthony SJ. Virus hunting. Virology. 2015; 479–480:194–9.
26. Docampo MD, Auletta JJ, Jenq RR. Emerging Influence of the Intestinal Microbiota during Allogeneic Hematopoietic Cell Transplantation: Control the Gut and the Body Will Follow. Biology of blood and marrow transplantation : Biol Blood Marrow Transplant. 2015; 21(8):1360–6.
27. Choi J, Goh G, Walradt T, Hong BS, Bunick CG, Chen K, et al. Genomic landscape of cutaneous T cell lymphoma. Nat Genet. 2015; 47(9):1011–9. [PubMed: 26192916]
28. Kim SM, Bhonsle L, Besgen P, Nickel J, Backes A, Held K, et al. Analysis of the paired TCR alpha- and beta-chains of single human T cells. PloS one. 2012; 7(5):e37338. [PubMed: 22649519]
29. Howie B, Sherwood AM, Berkebile AD, Berka J, Emerson RO, Williamson DW, et al. High-throughput pairing of T cell receptor alpha and beta sequences. Sci Transl Med. 2015; 7(301): 301ra131.
30. Tang F, Barbacioru C, Wang Y, Nordman E, Lee C, Xu N, et al. mRNA-Seq whole-transcriptome analysis of a single cell. Nat Methods. 2009; 6(5):377–82. [PubMed: 19349980]
31. Faherty SL, Campbell CR, Larsen PA, Yoder AD. Evaluating whole transcriptome amplification for gene profiling experiments using RNA-Seq. BMC Biotechnol. 2015; 15:65. [PubMed: 26223446]

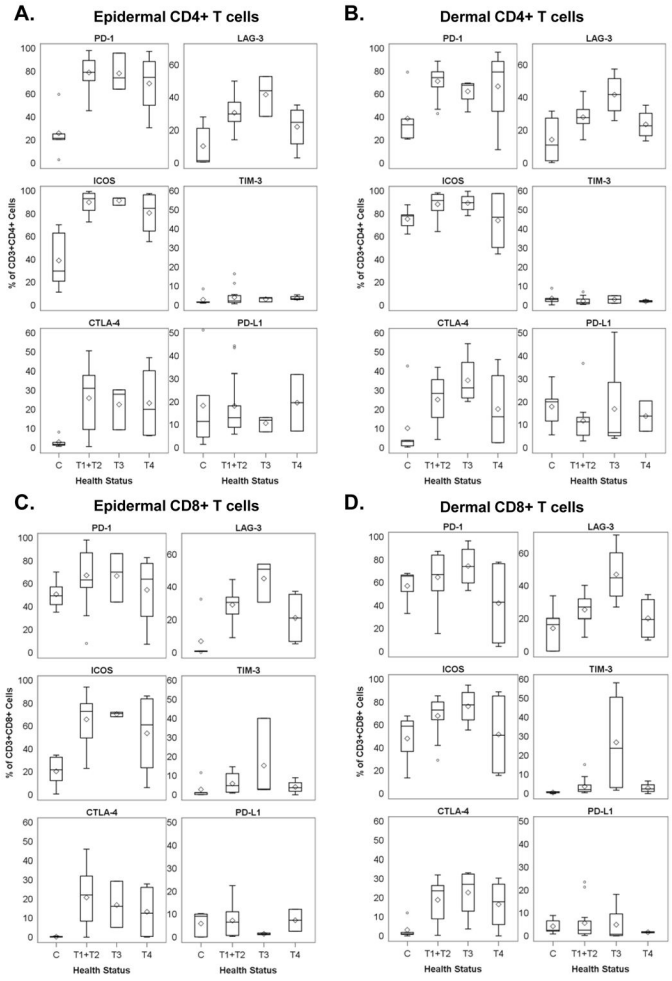

Figure 1. Immune checkpoint expression by $CD3^+CD4^+$ and $CD3^+CD8^+$ T cells

(A) Percentage of $CD3^+CD4^+$ epidermal cells stained with the indicated immune checkpoint markers. **(B)** Percentage of $CD3^+CD4^+$ dermal cells stained with the indicated immune checkpoint markers. **(C)** Percentage of $CD3^+CD8^+$ epidermal cells stained with the indicated immune checkpoint markers. **(D)** Percentage of $CD3^+CD8^+$ dermal cells stained with the indicated immune checkpoint markers. C, controls; T1, patches/plaques < 10% of body surface area; T2, patches/plaques ≥ 10% of body surface area; T3, ≥ 1 skin tumor; and T4, erythroderma. Diamonds indicate the mean value; boxes span the 25th–75th percentile (inter-quartile range, IQR); whiskers indicate the highest/lowest data point within 1.5 * IQR from the box. Any remaining data points are shown as circles. The Kruskal Wallis test determined the indicated *P* values, which compare healthy control skin vs all tumor stages combined. There were too few samples from patients with T3 or T4 disease to discern true differences between tumor stages. See also Table 2. Representative data from 3 independent experiments are shown.

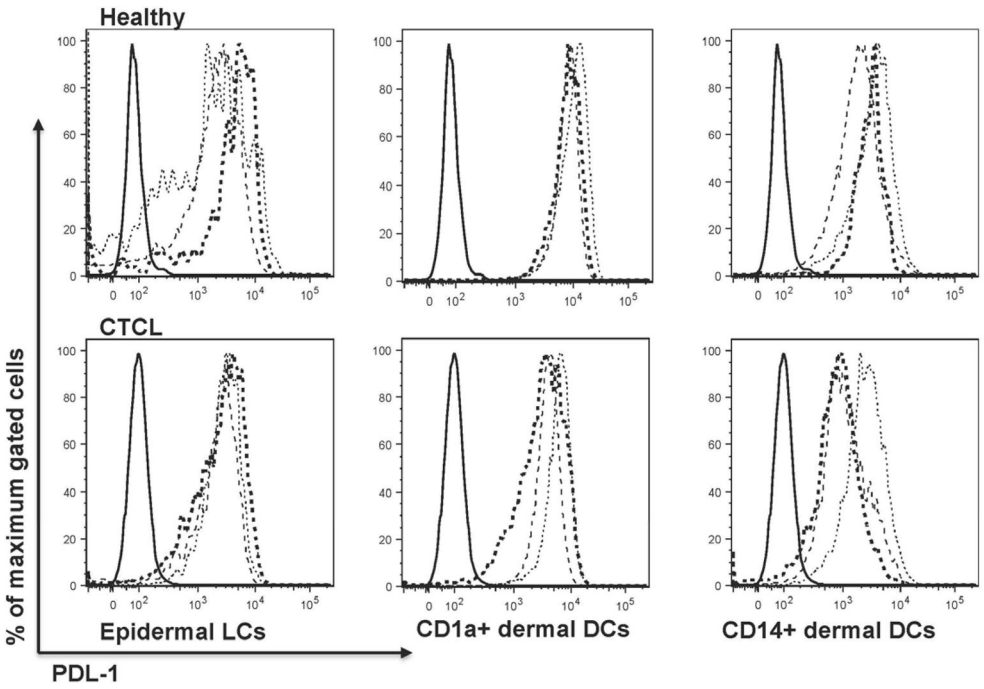

PD-L1 Median Fluorescent Intensity			
	Healthy (n=3)	CTCL (n=3)	*P* Value
Epidermal LCs	3781 ± 1708	2927 ± 288	>0.99
CD1a+ dermal DCs	9686 ± 1734	4875 ± 1649	0.1
CD14+ dermal DCs	3361 ± 791	1553 ± 911	0.1

Figure 2. PD-L1 expression by dendritic cell subsets from lesional CTCL and healthy skin

Flow cytometry histograms of PD-L1 expression from 3 healthy skin (top row) and 3 CTCL patients (bottom row). In each panel the solid histogram represents unstained controls, and the dotted lines each represent one of 3 lesional CTCL or healthy skin samples. The gating parameters were as follows: epidermal LCs ($CD1a^+$, $CD14^{neg}$, $HLA\text{-}DR^{bright}$), dermal $CD1a^+$ DCs ($CD1a^+$, $CD14^{neg}$, $HLA\text{-}DR^{bright}$, $CD11b^+$, $CD11c^+$), and dermal $CD14^+$ DCs ($CD1a^{neg}$, $CD14^+$, $HLA\text{-}DR^{bright}$, $CD11b^+$, $CD11c^+$). The Mann-Whitney *U* test was used to calculate the *P* values. Data are from one independent experiment.

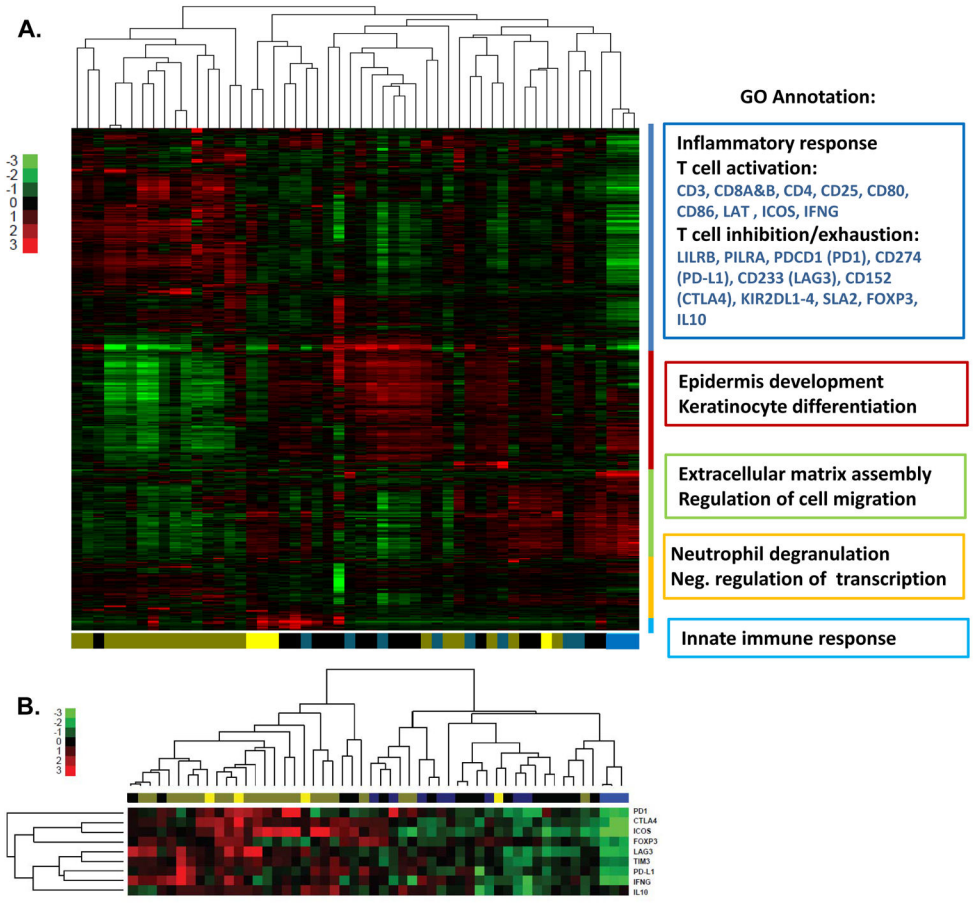

Figure 3. Unsupervised clustering heat map of genome-wide mRNA expression profiles, using skin samples from 49 MF/SS patients and 3 healthy individuals

(A). The unsupervised hierarchical clustering analysis identified a distinctive mRNA expression pattern for early stage MF (T1/T2) compared with advanced stage MF/SS (T3/T4) samples, and both groups are different from healthy skin. Data shown are log2 transformed expression values relative to the mean expression level across all samples of 6,418 genes (see Materials and Method for details). Genes in rows and samples in columns were both hierarchically clustered, while samples were color-coded by sample type. The following sample categories were assigned by color: healthy control (light blue), T1 stage (blue), T2 stage (black), T3 stage (ochre) and T4 stage (yellow). The gene ontology (GO) analysis identified five clusters. The GO annotation for each cluster of genes shows their related functions and were associated with 1) an immune/inflammatory response (T-cell activation and dysregulation/exhaustion) signature, 2) epidermis and keratinocyte development, 3) extracellular matrix and cell migration regulation, 4) neutrophil degranulation and negative regulation of transcription and 5) innate immune response. (B) To elucidate whether MF/SS display a distinctive exhaustion-related marker expression profile compared with healthy skin, we performed a supervised analysis following the previously mentioned criteria. Immune checkpoint and inflammatory gene expression profiling [PDCD1 (PD-1), CD274 (PD-L1), HAVCR2 (TIM3), CTLA4, LAG3, ICOS, IFNG, FOXP3 and IL10] was performed. Clustering analysis divided CTCL skin samples

into 2 groups based on decreased/inactivated and increased/highly activated expression of gene sets associated with immune checkpoint inhibition. Advanced stages (T3/T4) displayed higher expression of immune checkpoint and inflammation genes than did T1/T2 stage patients or healthy controls. One independent experiment was performed with 45 CTCL patients and three healthy controls.

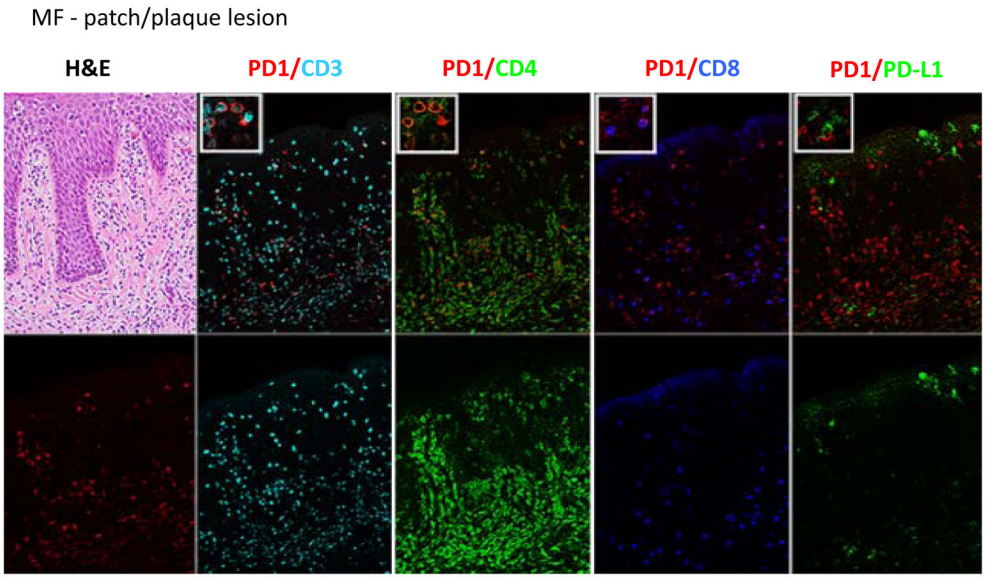

Figure 4. Histologic and immunophenotypic features of CTCL plaque, with 6-color multiplex immunohistochemistry for immune checkpoint expression

Multiplex images performed on skin sections of MF lesion from a representative patient with plaques (T2) is shown. PD-1 co-localizes with CD3, CD4, and CD8 expression. PD-1 and PD-L1 expression do not overlap. [200x magnification; insets represent 400x magnification of small regions of multiplex images]. Representative data from 3 independent experiments are shown.

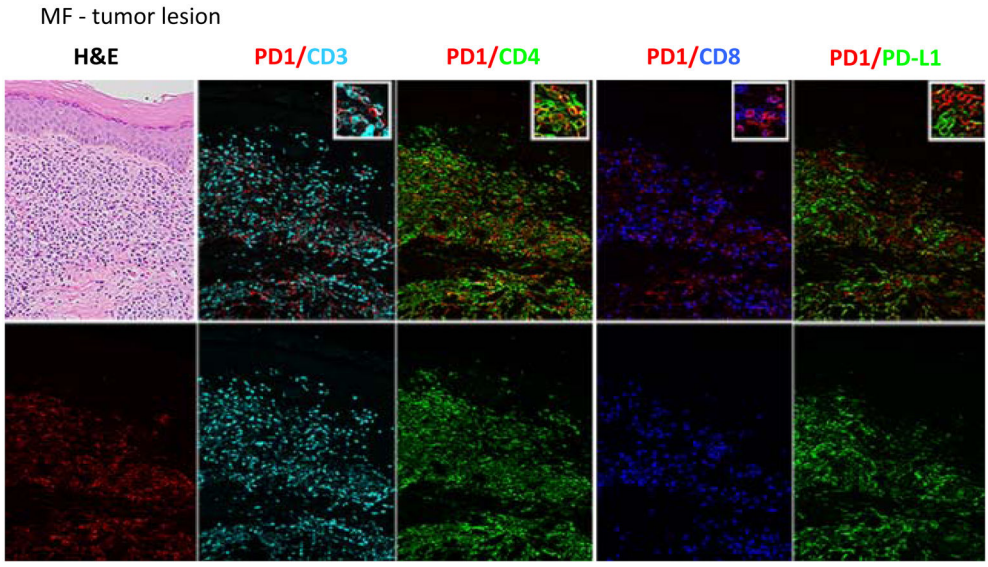

Figure 5. Histologic and immunophenotypic features of CTCL tumor, with 6-color multiplex immunohistochemistry for immune checkpoint expression

Multiplex images performed on skin sections of MF lesion from a representative patient with tumor lesion (T3) is shown. PD-1 co-localizes with CD3, CD4, and CD8 expression. PD-1 and PD-L1 expression do not overlap. Higher expression of PD-1 and PD-L1 expression is noted on tumor lesion (T3), compared with plaque (T2, Fig. 4). [200x magnification; insets represent 400x magnification of small regions of multiplex images]. Representative data from 3 independent experiments are shown.

Table 1

Demographic characteristics of the CTCL patient population (n = 37) studied using T-cell and DC émigrés from skin explant cultures of epidermal and dermal lesional skin.

Age (years)	
Median (range)	57 (24–86)
Gender	
Male	23
Female	14
Race/Ethnicity	
Caucasian	28
African-American	4
Hispanic	3
Unknown	2
Clinical Stage	
IA	9
IB	11
IIA	1
IIB	7
IIIB	3
IVA	5
IVB	1

Table 2

Percentages of epidermal and dermal $CD3^+$ T cells among the émigrés from skin explant cultures of lesional skin expressing immune checkpoint markers.

Cell Subset	Marker	Control		CTCL		*P* value
		Median	Range	Median	Range	
$CD4^+$ Epidermis	PD-1	21.80	(2.86–60.00)	77.90	(30.7–98.30)	**0.001**
	LAG-3	1.46	(0.56–28.10)	29.55	(3.15–52.9)	**0.007**
	ICOS	29.90	(11.40–70.40)	93.60	(55.70–99.70)	**0.001**
	TIM-3	1.53	(1.03–8.57)	3.00	(0.77–16.50)	0.25
	CTLA-4	1.68	(0.71–8.14)	29.25	(0.59–50.70)	**0.005**
	PD-L1	11.48	(1.43–51.40)	12.85	(5.91–44.40)	0.68
$CD4^+$ Dermis	PD-1	33.30	(21.04–79.40)	72.60	(11.8–96.9)	**0.031**
	LAG-3	11.07	(0.36–31.70)	27.70	(13.6–57.5)	0.055
	ICOS	78.30	(62.40–88.10)	91.80	(45–99.9)	0.051
	TIM-3	3.05	(0.16–8.95)	1.73	(0.43–7.05)	0.4
	CTLA-4	3.31	(0.34–42.80)	28.60	(2.57–54.5)	0.055
	PD-L1	20.10	(5.61–31.10)	9.12	(2.97–50.5)	0.2
$CD8^+$ Epidermis	PD-1	49.50	(35.20–70.40)	66.90	(7.41–98.40)	0.11
	LAG-3	0.77	(0.08–32.58)	30.90	(5.45–54.10)	**0.008**
	ICOS	21.80	(0.68–34.78)	72.50	(6.25–94.40)	**0.004**
	TIM-3	1.02	(0.07–11.58)	3.69	(0–40.20)	0.08
	CTLA-4	0.00	(0–0.56)	21.60	(0–46.10)	**0.004**
	PD-L1	9.17	(0–10.30)	2.82	(0.34–22.60)	0.68
$CD8^+$ Dermis	PD-1	65.80	(33.10–68.12)	67.20	(4.43–96.70)	0.37
	LAG-3	16.50	(0.19–34.00)	27.50	(7.01–71.30)	0.09
	ICOS	59.10	(13.70–68.00)	73.40	(15.9–95.10)	**0.048**
	TIM-3	0.47	(0–1.01)	2.57	(0–58.30)	**0.006**
	CTLA-4	1.03	(0–12.10)	23.70	(0–33.20)	**0.018**
	PD-L1	2.50	(0.84–8.95)	1.80	(0–23.60)	0.52

P values from the Wilcoxon rank sum test reflect comparison of the percentage of cells from healthy versus diseased skin expressing each marker.